Structural behaviour of octagonal tubular steel stub columns under uniaxial compression

J.Y. Zhu & T.M. Chan
Department of Civil and Environmental Engineering, The Hong Kong Polytechnic University, Hung Hom, Hong Kong

B. Young
Department of Civil Engineering, The University of Hong Kong, Hong Kong

ABSTRACT: This paper presents the experimental and numerical investigations on the compressive behaviour of cold-formed steel tubular stub columns with octagonal cross-section. Companion stub columns with circular and square cross-sections were also examined and compared. The material properties, dimensions and geometric imperfections for each specimen were carefully measured. Load-deformation relationships and failure modes of the test specimens were presented. Finite element methodology was also developed and validated against the experimental results. The current design codes from Europe and North America were assessed.

1 INTRODUCTION

Polygonal steel tubes have been proved as a very popular structural member in transmission poles and telegraph towers (Slocum 2015). To achieve an economical design in such structures, the width to thickness ratio (cross-section slenderness) should be optimized. Numerous investigations have been conducted on the local buckling behaviour of tubular steel with polygonal cross-sections. Aoki et al. (1991), Godat et al. (2012) and Tran et al. (2016a) conducted experimental investigations on hexagonal, octagonal and hexadecagonal tubular stub columns. Migita & Fukumoto (1997) and Teng et al. (1999) carried out numerical investigations on the critical local buckling stress of steel tubular members with polygonal cross-section. Finite element model was established by Goncalves and Camotim (2013) and Tran et al. (2016b). However, the abovementioned studies mainly focused on thin-walled tubular sections with Class 4 cross-sections.

To extend the study to Class 1-3 cross-sections, this paper presents both experimental and numerical investigations on tubular steel stub columns with Class 1-3 cross-sections. The experimental study includes three different cross-section shapes. In additional to octagonal cross-section, two commonly adopted cross-section shapes circular and square were investigated for comparison. Companion finite element analysis were conducted and validated by the experimental results. Cross-section slenderness limit based on the current code of practice Eurocode 3 (EN 1993-1-1, 2005) and ASCE standard (ASCE/SEI 48-11, 2011) were assessed by the structural performance data. In accordance with the assessment, the cross-section slenderness of octagonal section was discussed.

2 EXPERIMENTAL INVESTIGATION

In the present study, three tubular steel stub columns with cross-section shapes of octagonal, circular and square were tested under monotonic axial compression. The nominal yield stress of the steel tubes is 355 MPa. The octagonal steel tubes were fabricated by welding two cold formed half-section. The cold-formed steel plates were bent by the press-braking method. Similar method was applied to the circular and square steel tubes for consistency. The octagonal specimen was labelled as OctHS while CHS and SHS stand for circular and square specimens respectively. The dimensions of the cross-section for each specimen were precisely measured by a digital caliper with an accuracy of 0.01 mm and was summarized in Table 1 where b is the width of the octagonal and square cross-sections as shown in Figure 1; D is the outer diameter of the circular section; t is the tube thickness; w_{max} is the maximum local imperfection. The dimension of the circular section was designed from the circumscribed circle of the octagonal cross-section. The height of all the specimens are 700 mm.

Table 1. Dimension of the specimens.

Specimen	*b or D*	*t*	*b/t or D/t*	w_{max}	w_{max} /*t*
	mm	mm		mm	
OctHS	55.8	5.55	10.1	1.23	0.22
CHS	199.8	5.96	33.5	2.00	0.34
SHS	189.4	5.92	32.0	0.33	0.06

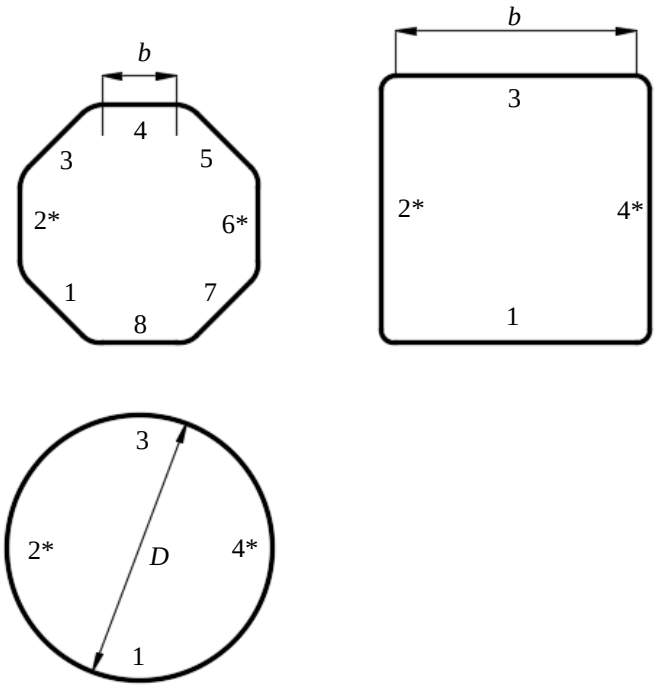

Figure 1. Dimensions of OctHS, CHS and SHS.

2.1 *Geometric local imperfection*

The geometric local imperfection in terms of deviation from a plane surface for all the specimens was measured over the height of each specimen before the test. Figure 2 shows the set up for the imperfection measurement. The specimen was placed on a milling machine. For specimens OctHS and SHS, three LVDTs were mounted on the milling machine in the orthogonal direction to record the imperfection at the mid-portion and two corner-portions of each face as shown in Figure 2. For specimen CHS only one LVDT was mounted in the orthogonal direction. The local imperfection was calculated as $(d_1+d_3)/2-d_2$ where d_1, d_2 and d_3 are the measured displacement from LVDT 1, 2 and 3 (Fig. 2). The initial readings at both ends of the specimen were regarded as reference points and other readings were adjusted in relation to the reference points to eliminate the error from the initial tilting of the tube. Figure 3 shows the recorded imperfection profile of all specimens (+ve is outwards and –ve is inwards). The surface number with asterisk indicates the location of welded joint. A bow shaped imperfection profile was found in the surfaces containing welded joint and the surface 90° apart from them in the specimens OctHS and CHS whilst this observation was not found in specimen SHS. This indicated the welding process may cause such an imperfection profile on steel tubes with octagonal and circular cross-sections. The magnitude of the maximum measured imperfection, w_{max}, and the ratio between the maximum imperfection and the tube thickness was summarized in Table 1.

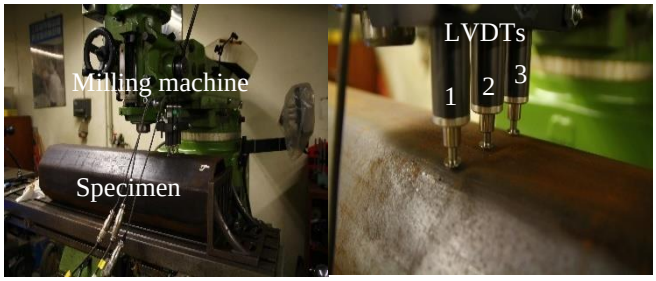

Figure 2. Set up of imperfection measurement.

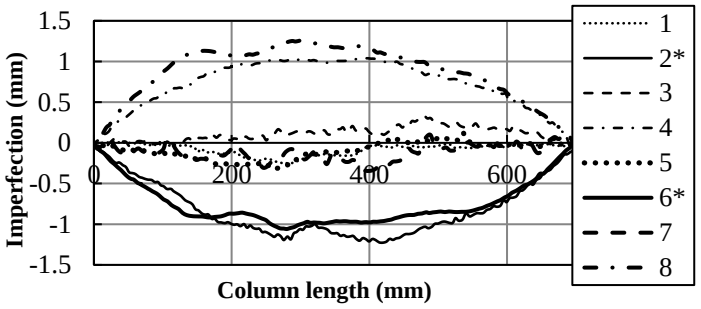

(a) OctHS

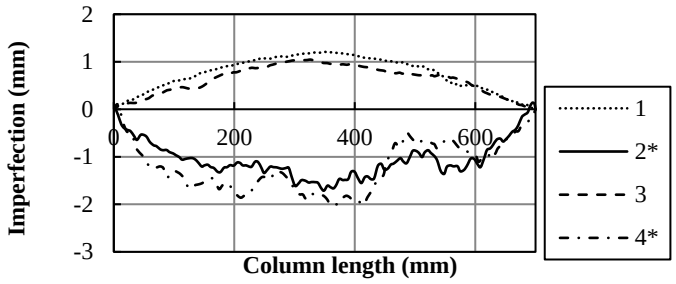

(b) CHS

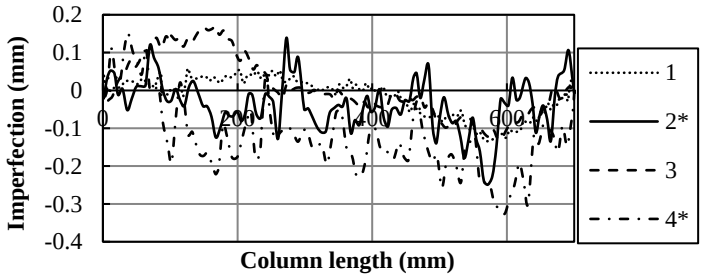

(c) SHS

Figure 3. Imperfection profiles.

2.2 *Tensile coupon tests*

The material properties of steel tubes were examined through the tensile coupon tests. In this investigation, two flat steel coupons were extracted from the flat side for each steel tube with octagonal and square cross-section shape and two curved coupons were extracted from the circular tube. The dimension of the flat steel coupon was designed in accordance with the BS EN ISO 6892-1 (2009) while the dimension of the curved coupons was designed in accordance with Ma et al. (2015). The tensile coupon test was conducted

using a MTS machine with a load capacity of 50 kN. To capture the static stress-strain curves, the test was paused for 100 seconds near the yield stress and near the ultimate stress. The adopted loading rate was 0.05 mm/min before 0.2% of strain and 0.5 mm/min after that until fracture (Huang and Young, 2014). Extensometers with 25 mm and 50 mm gauge length were used for curved coupon and flat coupon respectively. The test results are shown in Table 2, where $\sigma_{0.2}$ is the 0.2% proof stress; σ_u is the ultimate tensile stress of steel coupon; E_s is the Young's modulus; ε_{25mm} and ε_{50mm} are the fracture elongation based on the extensometer with gauge length of 25 mm and 50 mm respectively. ε_f is the elongation at fracture based on the original gauge length which is calculated from BS EN ISO 6892-1 (2009), $5.65\sqrt{S_0}$ where S_0 is the cross-sectional area of the steel coupon. The elongation based on the original gauge length was measured by re-matching the fracture pieces of the coupon. It can be found that all the fracture elongations satisfied the ductility requirement (>15%) in Eurocode 3 (EN 1993-1-1, 2005).

Table 2. Material properties of steel specimens.

Tensile coupon	$\sigma_{0.2}$	σ_u	E_s	ε_{25mm} or ε_{50mm}	ε_f
	MPa	MPa	GPa	%	%
OctHS	384	505	217	27.9	33.8
CHS	453	583	216	31.1	31.1
SHS	478	569	221	28.1	32.5

2.3 *Stub column tests*

The stub column tests were conducted using a MTS machine with a load capacity of 4600 kN. The arrangement of instrumentation is shown in Figure 4. For octagonal and square specimens (OctHS and SHS), strain gauges were attached at four flat sides and four corners to measure the axial strain. For the circular tube (CHS), strain gauges were attached on the surfaces at 90° to each other. The axial strain measured by the strain gauge was used to evaluate the 0.2% proof stress of the steel tubes. Four LVDTs with a measuring range of 50 mm and an accuracy of 0.1 mm were installed around the specimens to monitor the axial end-shortening. Each end of specimens was confined by a steel ring to prevent the elephant's foot buckling at the ends of specimens. Figure 4 shows the set-up for the specimens CHS. The load rate was maintained at 0.3 mm/min. To capture the static stress-strain curves, same arrangement as in the tensile coupon test was adopted.

The test results for the stub column tests are summarized in Table 3, where N_u is the load capacity of the specimens; $\sigma_{0.2,\,sc}$ is the 0.2% proof stress for the stub hollow steel tubes; $\sigma_{u,\,sc}$ is the ultimate stress for the stub hollow steel tubes. From the $\sigma_{u,\,sc}/\sigma_{0.2}$ value in Table 3, it can be found the ultimate stress of the steel tube with square cross-section marginally reaches the yield stress obtained from the tensile coupon test ($\sigma_{u,\,sc}/\sigma_{0.2}$ = 0.99). It is noted that the *b/t* ratio of the square cross-section (*b/t* = 32.0) is higher than the suggested maximum value for Class 1 to 3 cross-sections ($b/t \leq 29.4\varepsilon$) in Eurocode 3 and the upper limit of *b/t* value ($b/t \leq 31.1$) for the condition $f_u \geq f_y$ in ASCE standard (2011) where f_u and f_y are the ultimate stress and yield stress of steel member. The *b/t* ratio of the specimen OctHS (*b/t* = 10.1) and *d/t* ratio of the specimen CHS (d/t=33.5ε) are both satisfied the mentioned limits in Eurocode 3 (EN 1993-1-1, 2005) ($b/t \leq 32.9\varepsilon$ & $d/t \leq 46.7\varepsilon$) and ASCE standard (ASCE/SEI 48-11, 2011) ($b/t \leq 34.8\varepsilon$ & $d/t \leq 57.9\varepsilon$).

The normalized axial stress-axial strain relationships of the specimens are shown in Figure 5. The y-axis indicates the axial stress of the specimens over the yield stress $\sigma_{0.2}$ from the tensile coupon test. The x-axis indicates the axial strain converted from the axial end-shortening. It can be observed that both the strength hardening behaviour and ductility of the hollow steel tubes OctHS are better than that of the specimens CHS. The low strength hardening ratio and the ductility of the specimen CHS after yielding may be caused by the large imperfection to thickness ratio (*w/t* = 0.34) which is much larger than that in the specimen OctHS (*w/t* = 0.22).

The failure mode of each specimen was shown in Figure 6. It was observed that local buckling happened at the surface with welding joint first during the test for specimens OctHS and CHS, it may attribute to the large imperfection in that surface. The post-peak buckling mode of octagonal specimen is similar to a cylindrical shell buckling which may be caused by the bow-shaped geometrical imperfection.

Table 3. Results of stub column test.

Stub column	N_u	$\sigma_{0.2,\,sc}$	$\sigma_{u,\,sc}$	$\sigma_{0.2,sc}/\sigma_{0.2}$	$\sigma_{u,sc}/\sigma_{0.2}$
	kN	MPa	MPa		
OctHS	1470	408	471	1.06	1.23
CHS	1830	493	504	1.09	1.11
SHS	2210	---	471	---	0.99

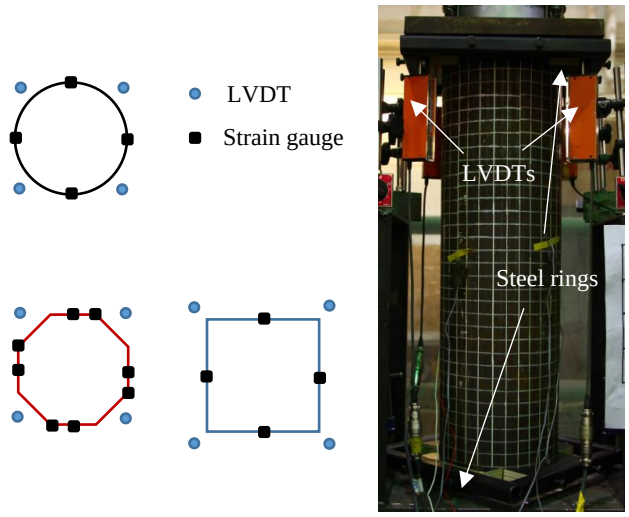

Figure 4. Instrumentations arrangement.

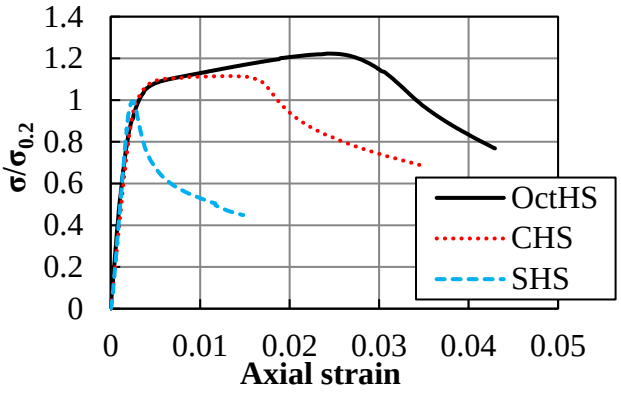

Figure 5. Normalized stress versus strain curves of the stub hollow tubes.

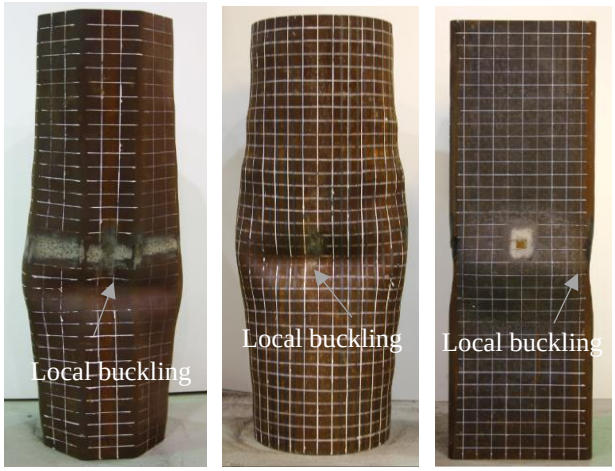

(a) OctHS (b) CHS (c) SHS

Figure 6. Failure modes for the stub hollow tubes.

3 FINITE ELEMENT ANALYSIS

3.1 *Model description*

A finite element (FE) analysis was conducted with the use of the commercial software package ABAQUS. The results of the tensile coupon tests were used for defining the material properties of steel in FE analysis. Four-node shell element with reduced integration, S4R was used in the analysis. Chan and Gardner (2008) and Ma et al. (2015) have successfully adopted this type of element in FE model of stub hollow steel tubes under compression. Full 3D model was established for all the specimens. The bottom of the column was constrained in all degrees of freedom (fix end). The top surface of the column was coupled to a reference point which was also constrained in all degree of freedom except axial direction. Load was applied to the reference point by imposing an axial displacement. Mesh convergence studies was conducted to determine the appropriate mesh configuration.

3.2 *Imperfection profile*

To capture both the axial load-shortening curves and the failure modes of the specimens in the experimental investigation. The measured imperfection profile was applied to the finite element model. For the specimens OctHS and CHS, the bow shaped imperfection profile was found in the surfaces containing welded joint and the surface 90° apart from them. The input imperfection profile in ABAQUS is the superposition of a half sine curve with the measured maximum imperfection amplitude and the buckling mode pattern from buckling analysis of eigenvalue with three different imperfection amplitudes: $t/10$, $t/50$ and $t/100$. For the model of specimen SHS, only the first buckling mode pattern with imperfection amplitudes: $t/10$, $t/50$ and $t/100$ was used.

3.3 *Validation*

The test results of the current experimental investigation and test result of one Class 4 octagonal specimens from Godat et al. (2012) were used to validate the finite element model. The imperfection profile for the specimens from Godat et al. (2012) was taken as the first buckling mode pattern with amplitudes of $t/100$, $t/50$ and $t/10$. Table 4 shows the FE results of load-carrying capacity. It can be found that the FE model underestimate the load capacity of specimens OctHS. This is due to the cold-forming enhancement at the corners which cannot be captured by the used material model from the tensile coupon in the flat zone of tubes. The load capacity of specimen CHS, on the other hand can capture the experimental findings well. The models with the imperfection amplitude of $t/100$ give the best prediction of load capacity on the specimens CHS, OctHS and SHS. For the Class 4 specimen OCT-1-A from Godat et al. (2012) the FE model with imperfection amplitude of 0.2 ($t/10$) can capture the load capacity well ($N_{u,FE}/N_u$=1.05).

Figure 7 shows the axial load - shortening curves of the FE simulations. It can be found the amplitude of the accompanying imperfection profile (buckling mode pattern) affects the post-yielding behaviour. However, the influence on the load-shortening curves are negligible when the amplitude changes from $t/100$ to $t/50$. Figure 8 shows the predicted failure mode for the test specimens.

Table 4. FE results of load-carrying capacity.

Specimens	Imperfection (mm)	$N_{u,FE}$ (kN)	$N_{u,FE}/N_u$
OctHS	0.06 ($t/100$)	1393	0.95
	0.11 ($t/50$)	1388	0.94
	0.55 ($t/10$)	1329	0.90
CHS	0.06 ($t/100$)	1792	0.98
	0.12 ($t/50$)	1790	0.98
	0.60 ($t/10$)	1766	0.97
SHS	0.06 ($t/100$)	2242	1.01
	0.12 ($t/50$)	2265	1.02
	0.60 ($t/10$)	2104	0.95
OCT-1-A (Godat et al. 2012)	0.02 ($t/100$)	378	1.15
	0.04 ($t/50$)	374	1.14
	0.20 ($t/10$)	343	1.05

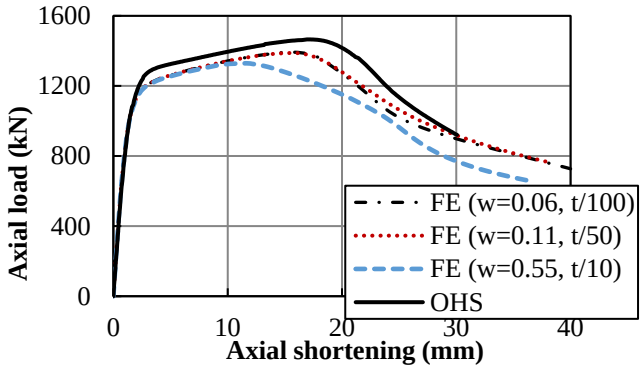

(a) OctHS

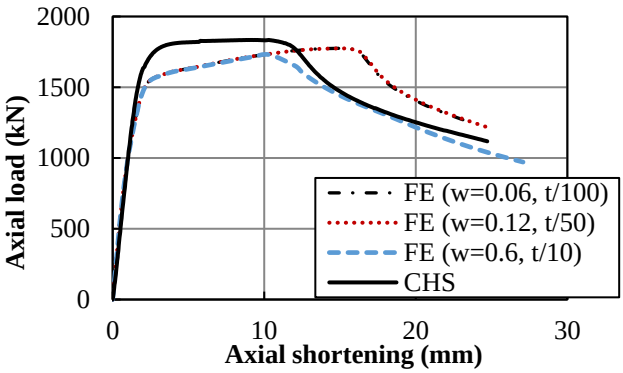

(b) CHS

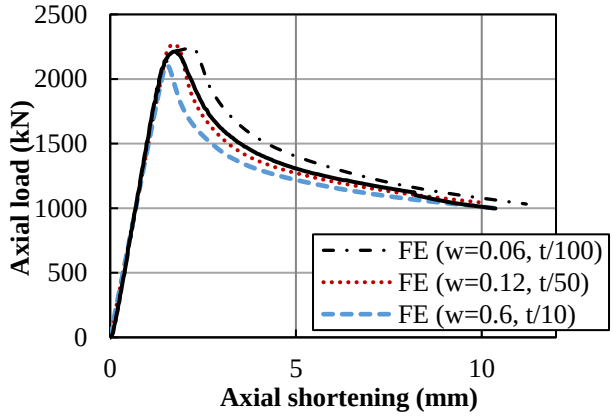

(c) SHS

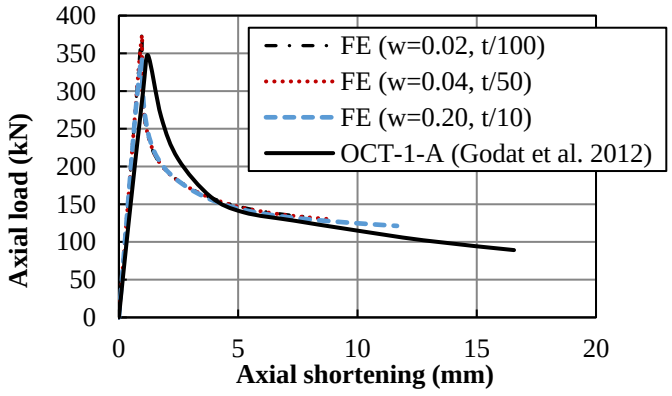

(d) OCT-1-A (Godat et al. 2012)

Figure 7. FE predictions of axial load-shortening curves.

Figure 8. FE predictions of failure modes.

4 DESIGN ASSESSMENT

The current cross-section classification system for octagonal cross-section under pure compression were assessed. The verified finite element model was used to generate further data for stub columns with octagonal cross-section for assessment. The material properties from the specimen OctHS were used in the additional FE models.

4.1 *Current cross-section classification system*

For columns under axial compression, the primary concern is the occurrence of local buckling before the yielding of steel tube. For the cross-section classification under pure compression, the cross-section with an ultimate stress that can reach the yield stress are considered as Class 1-3, whilst those where local buckling happened in the elastic stage before the yield stress are considered as Class 4. Eurocode 3 (EN 1993-1-1, 2005) provides the limiting proportions for the cross-section Class 1-3 of circular and rectangular cross-section as follows:

$$D/t \leq 90\,(235/f_y) \quad (1)$$

$$b/t \leq 42\sqrt{(235/f_y)} \quad (2)$$

where D is the outer diameter of circular cross-section; b is the width of rectangular section and t is the thickness. It is noted that octagonal cross-section is not specified in Eurocode 3 (EN 1993-1-1, 2005).

ASCE standard (ASCE/SEI 48-11, 2011) also provides the limitation of cross-section slenderness for Class 1-3 cross-sections as follows:

$$D/t \leq 6.9\,(3800/f_y) = 111.6\,(235/f_y) \quad (3)$$

$$b/t \leq 2.62\,(260/\sqrt{f_y}) = 44.4\sqrt{(235/f_y)} \quad (4)$$

ASCE standard also extends the limitation for b/t ratio to octagonal and hexagonal members. These two current codes of practice on cross-section classification were assessed by the existing experimental data and the accompanying finite element analysis results in the next section.

4.2 *Assessment*

The experimental results of Aoki et al. (1991) and Godat et al. (2012) on octagonal tubular steel stub columns were adopted for the assessment. The test results and additional finite element analysis data are listed in Table 5. Figure 9 shows the relationship between test/FE results ($\sigma_{u,sc}/\sigma_{0.2}$) and $b/[t\sqrt{(235/f_y)}]$ for octagonal steel tubular stub columns. From Figure 9, it can be observed that the current two limits in Eurocode 3 (42), and ASCE standard (44.4) may need to be further tightened to achieve optimum design.

As the shape of octagonal cross-section is between circular and rectangular cross-section, it is intrinsic to use equivalent circle approach for design assessment. In current study, three different equivalent circular cross-sections were adopted. D_o and D_i are the circumscribed and the inscribed diameter of octagonal cross-section respectively, D_p is the diameter of the equivalent circle with the same perimeter of the octagonal cross-section. Figure 10 shows the normalized ultimate strength (f_u/f_y) against $D/[t(235/f_y)]$. The corresponding limits in Eurocode 3 (90) and ASCE standard (111.6) are also shown in the Figure. It can be observed that in both three figures, there is no significant difference among three equivalent circle definitions. The trend suggests both Eurocode 3 and ASCE limits could be adequately adopted. Based on the current investigation, it is proposed an equivalent circle could be used for the design of octagonal cross-section based on Eurocode 3 and ASCE standard.

Table 5. Comparison between design limit and existing data.

Specimens	b	t	$\sigma_{0.2}$	$\sigma_{u,sc}$	b/t	$\sigma_{u,sc}/\sigma_{0.2}$
	mm	mm	MPa	MPa		
Aoki et al. (1991)						
OCT-15	147	4.50	289	278	32.7	0.96
OCT15-b	148	4.50	289	274	32.9	0.95
OCT-15w	150	4.50	289	275	33.3	0.95
OCT20-A	196	4.49	289	244	43.7	0.84
OCT25-A	264	4.52	289	206	58.4	0.71
OCT30	296	4.51	289	173	65.6	0.60
Godat. et al. (2012)						
OCT-1-A	95	1.90	279	210	50.0	0.75
OCT-4-A	75	1.37	265	225	54.7	0.85
Present study (Experiment)						
OctHS	56	5.50	384	471	10.2	1.23
Present study (FE)						
O185	59	1.85	384	354	31.9	0.92
O191	59	1.91	384	354	30.9	0.92
O200	59	2.00	384	363	29.5	0.95
O230	59	2.30	384	377	25.7	0.98
O240	59	2.40	384	380	24.6	0.99
O250	59	2.50	384	387	23.6	1.01
O260	59	2.60	384	390	22.7	1.02
O308	59	3.08	384	402	19.2	1.05
O324	59	3.24	384	406	18.2	1.06
O333	59	3.33	384	409	17.7	1.07
OctHS	56	5.5	384	447	10.2	1.17
OCT-1-A	95	1.9	279	221	50.0	0.79

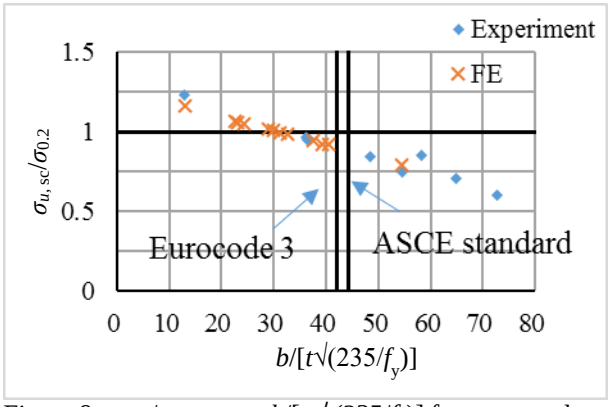

Figure 9. $\sigma_{u,sc}/\sigma_{0.2}$ versus $b/[t\sqrt{(235/f_y)}]$ for octagonal cross-section.

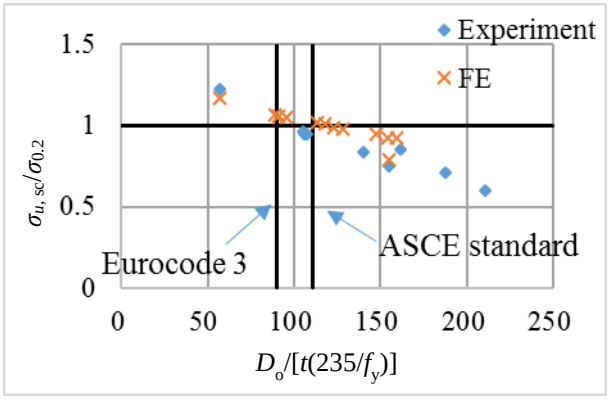

(a) D_o

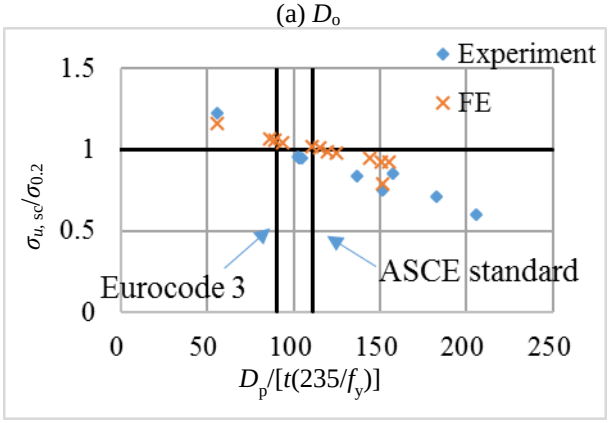

(b) D_p

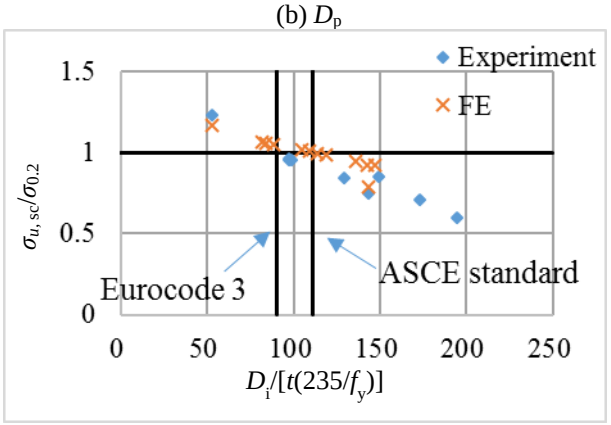

(c) D_i

Figure 10. $\sigma_{u,sc}/\sigma_{0.2}$ versus $D/[t(235/f_y)]$ for octagonal cross-section.

5 CONCLUSIONS

This paper presents the experimental and numerical investigations on the octagonal tubular steel stub columns. The geometrical imperfection was measured

and adopted in the finite element analysis. Finite element analysis captured well the experimental load carrying capacity and load-end shortening behaviour. The experimental results from current study and existing literature together with the additional data from finite element analysis were collated to assess the cross-section classification system in Eurocode 3 (EN 1993-1-1, 2005) and in ASCE standard (ASCE/SEI 48-11, 2011). The assessment shows the current slenderness limit (*b/t*) for octagonal cross-section in ASCE/SEI standard need to be tightened whilst the slenderness limit (*D/t*) in Eurocode 3, ASCE/SEI standards for circular cross-section can be used for octagonal cross-section with an equivalent circle's approach.

ACKNOWLEDGEMENTS

Authors are thankful to WoLee steel Co. Ltd. for supplying the test specimens. This study was also partly supported by the research funding from the Construction Industry Council under the project "Application of Polygonal High Strength Concrete-filled Composite Column in Seismic-resistant Buildings in Hong Kong". The support from the Chinese National Engineering Research Centre for Steel Construction (Hong Kong Branch) is also gratefully acknowledged.

REFERENCES

Aoki, T., Migita, Y. and Fukumoto, Y., 1991. Local buckling strength of closed polygon folded section columns. *Journal of Constructional Steel Research*, 20(4), pp.259-270.

ASCE/SEI 48-11. Design of steel transmission pole structures. Reston, Virginia: American Society of Civil Engineers; 2011

BSI (2005) BS EN 1993-1-1:2005: Eurocode 3 Design of steel structures, Part 1.1, General rules and rules for buildings. BSI, London, UK

BSI (2009) BS EN ISO 6892-1: Metallic materials: Tensile testing, Part 1: Method of testing at ambient temperature. BSI, London, UK.

Chan, T.M. and Gardner, L. 2008. Compressive resistance of hot-rolled elliptical hollow sections. *Engineering Structures* 30(2): 522–532.

Godat, A., Legeron, F. and Bazonga, D., 2012. Stability investigation of local buckling behavior of tubular polygon columns under concentric compression. *Thin-Walled Structures*, 53: 31-140.

Gonçalves, R. and Camotim, D., 2013. On the behaviour of thin-walled steel regular polygonal tubular members. *Thin-Walled Structures*, 62, 191-205.

Huang, Y. and Young, B. 2014. The art of coupon tests. *Journal of Constructional Steel Research* 96: 159-175.

Ma, J. L, Chan, T.M. and Young, B. 2015. Experimental investigation on stub-column behavior of cold-formed high-strength steel tubular sections. *Journal of Structural Engineering*, 142(5): p. 04015147-1 to 04015147-11

Migita, Y. and Fukumoto, Y., 1997. Local buckling behaviour of polygonal sections. *Journal of Constructional Steel Research*, 41(2-3): 221-233.

Slocum, R.M., 2015. Considerations in the design and fabrication of tubular steel transmission structures. *Proceedings of the Fifteenth International Symposium on Tubular Structures - ISTS 15*, 27-29 May 2015, Rio de Janeiro, Brazil.

Teng, J.G., Smith, S.T. and Ngok, L.Y., 1999. Local buckling of thin-walled polygonal columns subjected to axial compression or bending. *Proceedings of The Second International Conference on Advances in Steel Structures 15–17 December 1999*, Hong Kong, China

Tran, A.T., Veljkovic, M., Rebelo, C. and da Silva, L.S., 2016a. Resistance of cold-formed high strength steel circular and polygonal sections—Part 1: Experimental investigations. *Journal of Constructional Steel Research*, 120, 245-257.

Tran, A.T., Veljkovic, M., Rebelo, C. and da Silva, L.S., 2016b. Resistance of cold-formed high strength steel circular and polygonal sections-Part 2: Numerical investigations. *Journal of Constructional Steel Research*, 125, 227-238.